Journal of
Ceramic Science
and Technology

J. Ceram. Sci. Tech., 07 [02] 203-208 (2016)
DOI: 10.4416/JCST2016-00004
available online at: http://www.ceramic-science.com

Influence of Interfaces on Crack Propagation through a Layered Refractory Loaded by Thermal Shock

J. Hein*, O. El Khatib, M. Kuna

Institute of Mechanics and Fluid Dynamics, TU Bergakademie Freiberg,
Lampadiusstrasse 4, D-09599 Freiberg, Germany

received January 10, 2016; received in revised form March 10, 2016; accepted April 15, 2016

Abstract

Layered structures have been suggested to improve the thermal shock resistance of refractories. Owing to the fast temperature increase of the outer surface, high thermal tensile stresses occur inside the refractory. Depending on the intensity of thermal shock and the material, cracks may arise and grow through and between the layers. To study the behavior of such a crack system and the influence of interfaces on it, a symmetrically layered strip is considered. The cracks through the layers and along the interfaces are modeled using cohesive zones. Systematic changes of the cohesive parameters and their consequences on crack growth through the layers of the strip are shown.

Keywords: Refractories, multilayer ceramics, thermal shock, cohesive zones, interfaces, crack growth

I. Introduction

Within the framework of the Priority Program SPP 1418 "FIRE" layered or functionally graded materials have been suggested as a way to improve the thermal shock resistance of refractories with minimized carbon content. The avoidance of carbon would improve the steel production process significantly, not just because of the lower CO and CO_2 emissions.

During the development and fabrication of layered structures based on thin tape-cast ceramic layers [1], the importance of the interface properties came into focus. Design in this respect influences the ability to properly fabricate layered ceramics without failure during the sintering process and also of the refractories to resist severe thermal shocks.

In response to sudden high temperature changes, high thermal tensile stresses arise and may lead to the formation of cracks. In layered structures, these cracks are able to branch from the bulk into the interfaces between the layers depending on the interface properties, which is also described by Lemaitre [2]. Because of this effect, a crack may arrest and failure of the total structure can be obviated. Clegg *et al.* [3] described a simple way to create layered ceramics with weak interfaces by coating the layers with graphite. It was shown that this leads to substantially higher fracture energy.

Davis *et al.* [4] presented a fabrication method for multi-layered ceramics with porous interlayers for deflecting cracks. The big problem of finding suitable material has been pointed out with references to other studies. Fracture behavior of layered strips with textured layers has been studied by Pavlacka *et al.* [5] Crack deflection in these layers are shown in notched bars in bending tests. Harmer *et al.* [6] also briefly outlined different ways for improving ceramics. They listed methods like laminar ceramic-polymer composite designs, sandwich constructions with tougher surface layers, [7] structures consisting of inner layers with the ability to transform into a monoclinic phase for arresting cracks or the improvement of layered structures with residual stresses to compensate for stresses caused by loading. Lakshminarayanan and Shetty [8] used the phase transformation in the outer layers of a three-layered ceramic to create residual stresses. In other studies, these stresses are created by laminating materials with different thermal expansion coefficients [1, 10–17]. Bermejo *et al.* [18, 19] studied the influence of three different layer thickness ratios in symmetrically layered ceramics on their fracture behavior under bending. Thereby residual stresses due to phase transformation and different thermal expansion coefficients are calculated and experimentally determined by means of the indentation method.

Theoretical investigations on mixed mode loading of different cracks in layered structures and experimental setups are described by Hutchinson and Suo [20]. Lube *et al.* [13] determined the effective fracture toughness of laminates with residual stresses resulting from different thermal expansion coefficients of the layers. They calculated the stress intensity factor of an edge crack (depending on crack length) through the layers with a fracture mechanical weight function (for homogeneous material) and showed the effect of different thickness ratios of the layers, influence of ratio in Young's modulus and thermal expansion on the shielding effect (effective R-curve). Zhang, Telle and Uebel [21] used a discrete element model to study the damage of layered ceramics with weak interfaces as caused by three-point-bending. In this study the number of interfaces and their weakness were varied. Ševeček *et al.* [17] studied an in-plane

* Corresponding author: jarno.hein@imfd.tu-freiberg.de

edge crack in an alternating layered ceramic with residual stresses due to cooling down from sintering temperature (mismatch of thermal expansion coefficient). They varied the crack length and the layer thickness and predicted the onset and propagation of such a surface crack by analyzing the stresses and energy release rate of the crack calculated based on the *J*-integral. Investigations on bifurcation of a crack in layered ceramics with strong interfaces were performed in several studies [22–26]. In these studies, the influence of residual stress ratio of two neighboring layers on the bifurcation is shown and, on this basis, advice is given about the thickness of the compressive layers [24]. With regard to high-temperature shielding applications, thermal barrier coatings are studied in a wide range of investigations [27–39]. Optimizations of layered ceramics with regard to layer thickness and material order are performed by Hein *et al.* without [40] and with consideration of residual stresses [1,16] using an optimization method that combines Monte Carlo simulation and evolution strategies. However, these investigations were just based on continuum mechanics, so interface strength or any possibility of damage along interfaces or through layers (crack nucleation or propagation) were not taken into consideration.

In this study, a symmetrical layered strip is examined in order to study crack propagation through the layers and the branching of cracks into the interfaces caused by thermal shock. The question of how the strength of layers and interfaces affects crack growth is investigated. For this purpose, cohesive elements are used to model the possible crack path through the layers along the symmetry plane and along the interfaces.

II. Finite Element Simulation of Thermal Shock Behavior and Crack Propagation

A long strip (in x_3-direction) loaded by a sudden temperature change $\Delta T(x_1 = 0) = \overline{T} > 0$ K (rapid heating) on the entire left surface shows a thermal stress distribution $\sigma_{22}(x_1)$ of compression near the surfaces (left and right) and tensile stresses inside the strip [16, 40, 41]. The stresses depend on the material properties and the current temperature distribution. If they reach the critical material strength, damage occurs. To examine such behavior, a symmetrically layered strip is considered. This strip consists of Al_2O_3 (porosity $P = 25$ %) and MgO ($P = 30$ %) distributed in five layers in symmetrical order as shown in Fig. 1a (half model).

Assumptions are a sudden temperature jump of $\overline{T} = 400$ K on the loaded surface $x_1 = 0$ and a fixed temperature (initial temperature) on the surface $x_1 = W$, while all other boundaries have adiabatic boundary conditions. Furthermore, all boundaries are stress-free. Owing to symmetry, the strip can be modeled as a half model. Fig. 1b presents the temperature (blue lines) and stress (red lines) distribution at $t = 0.01$ s (dashed line) and at $t = 1$ s (solid line) caused by this thermal shock without consideration of residual stresses as done by Hein and Kuna [16].

Because of dominant stresses in x_2-direction, damage evolution in x_1-direction through the bulk material (along the symmetry plane) can be assumed. The realization of a damageable symmetry plane via cohesive contact/elements [42,43] in the finite element program Abaqus [44] is visualized in Fig. 2.

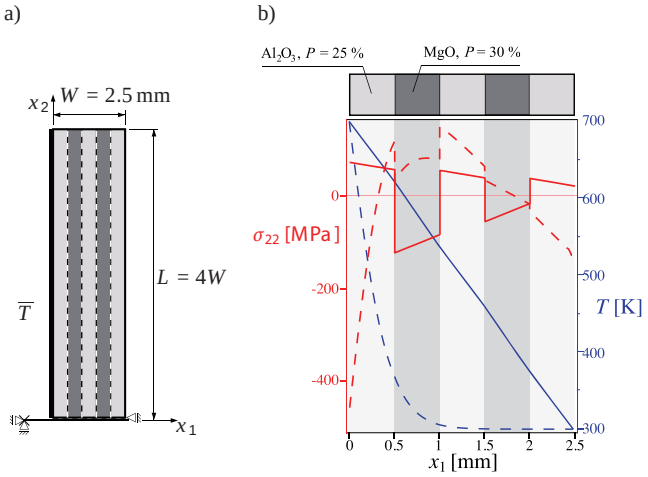

Fig. 1: Thermally shocked layered strip: (a) Half model; (b) Temperature (blue) and thermal stress (red) distribution at $t = 0.01$ s (dashed) and $t = 1$ s (solid).

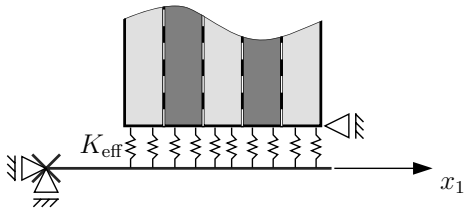

Fig. 2: Layered strip with cohesive contact to a rigid surface.

Thereby, the contact is defined between the half model of the layered strip and a fixed analytical rigid surface that is located in the symmetry plane. The contact definition is simplified by springs having an effective stiffness

$$K_{\text{eff}} = (1 - D)\, K, \tag{1}$$

which is given by the local damage variable $D \in [0, 1]$ and the stiffness K of the undamaged state. Here, the contact should follow locally the bilinear traction-separation-law as shown in Fig. 3.

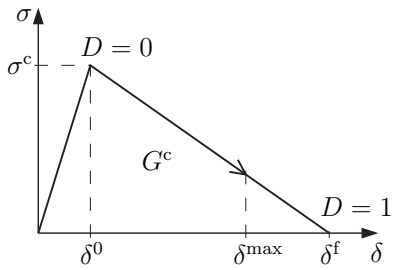

Fig. 3: Bilinear traction-separation-law of the cohesive contact.

Starting from undamaged state, the traction σ increases linearly with increasing separation δ

$$\sigma = K\,\delta \tag{2}$$

until the cohesive strength σ^c is reached. Then damage occurs ($D > 0$) until total damage ($D = 1$) is reached at a separation δ^f. Thereby, the tractions are given by

$$\sigma = K_{\text{eff}}\,\delta = (1 - D) K\,\delta. \tag{3}$$

The area below this traction-separation curve describes the cohesive energy G^c at total failure.

In the two-dimensional case, equation (2) can be written analogously with respect to tractions and separations in normal $(\cdot)_n$ and shear direction $(\cdot)_s$

$$\underline{\sigma} = \begin{pmatrix} \sigma_n \\ \sigma_s \end{pmatrix} \begin{pmatrix} K_{nn} & K_{ns} \\ K_{ns} & K_{ss} \end{pmatrix} \begin{pmatrix} \delta_n \\ \delta_s \end{pmatrix} = \underline{\underline{K}}\,\underline{\delta}. \tag{4}$$

Here, we assume an independent, uncoupled behavior in each direction. So, the stiffness K_{ns} vanishes. Also K_{ss} should be zero (or negligibly small, because of numerical reasons) to allow a free thermal expansion in x_1-direction. In this work, the influence of the interfaces on crack propagation is studied. So, the interfaces are also modeled with cohesive elements (dashed lines in Fig. 2). There, neither the stiffnesses in normal nor in shear direction can be neglected.

In Abaqus the damage variable is calculated by [44]

$$D = \frac{\delta^f (\delta^{max} - \delta^0)}{\delta^{max} (\delta^f - \delta^0)}, \tag{5}$$

where δ^{max} describes the maximum of separation the node has reached in the loading history until the current time step. However, this is equal to

$$D = 1 - \frac{\sigma^{max}}{\Sigma} \tag{6}$$

using tractions $\Sigma = K\,\delta^{max}$ that would exist in a model without damage. The mismatch to a desired definition

$$\tilde{D} = 1 - \frac{\sigma^{max}}{\sigma^c} \quad \text{with } \sigma^{max} = \sigma(\delta^{max}, D) \tag{7}$$

becomes obvious especially for very stiff cohesive elements (large K). To correct this, a description $\tilde{D} = \tilde{D}(D)$ can be found by using

$$\sigma^{max} = (1 - D) K \delta^{max} \tag{8}$$

in equation (7) to get δ^{max}, which should be plugged in equation (5). This way, the damage variable

$$\tilde{D} = \frac{D}{D + (1 - D)\,\lambda^f} \quad \text{with } \lambda^f = \frac{\delta^f K}{\sigma^c} \tag{9}$$

can be formulated [45].

III. Results and Discussion

Material parameters of MgO and Al_2O_3 with porosities of $P = 30$ % and $P = 25$ % are listed in Hein [16]. Parameters of the cohesive zones shown in Table 1 are chosen without experimental exploration on real ceramics. Default values are underlined.

To differentiate between interface parameters and bulk properties of MgO and Al_2O_3 the superscripts $(\cdot)^I$, $(\cdot)^M$ and $(\cdot)^A$ are used here.

Fig. 4 shows the damage evolution through the layers $\tilde{D}(x_1)$ along the symmetry plane at different times until the thermal steady state at $t = 1$ s is reached.

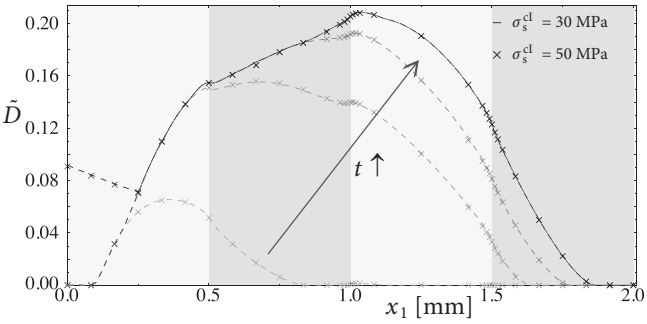

Fig. 4: Damage $\tilde{D}(x_1)$ at $\in$ {0.001, 0.005, 0.01, 0.1, 1}s due to $\bar{T} = 400$ K (Al_2O_3 and MgO bulk strength $\sigma^{cA} = \sigma^{cM} = 60$ MPa).

Thereby, the bulk strength of Al_2O_3 and MgO is $\sigma^{cA} = \sigma_n^{cA} = \sigma_s^{cA} = \sigma^{cM} = \sigma_n^{cM} = \sigma_s^{cM} = 60$ MPa, while the interface shear strength σ_s^{cI} is varied between 30 MPa (dashed line) and 50 MPa (cross symbols). As it can be seen, there is no effect of this variation on $\tilde{D}(x_1)$. Damage starts in the first layer near the first interface and grows mainly through the second and third layer until $t = 0.1$ s. Then, the damage increases just in the first layer. A maximum of $\tilde{D}(x_1)$ around 21 % near the second interface can be found.

To get full damage of cohesive zones through at least two layers, the thermal shock has to be increased to $\bar{T} = 700$ K as it can be seen in Fig. 5 in comparison to Fig. 4.

Fig. 5 illustrates, how damage of the first interface influences damage $\tilde{D}(x_1)$ through the bulk at different times. Thereby, the interface shear strength is set to be $\sigma_s^{cI} = 30$ MPa.

The damage evolution is similar to the weaker thermal shock, but with total failure $\tilde{D} = 1$ of the second and third layer at $t = 0.1$ s. The damage of the bulk in earlier time steps is similar to the bulk damage without considering the first layer to be damageable (solid line). Reaching nearly the thermal steady state at $t = 1$ s, the damage of the first interface leads to an additional failure of the first layer (dashed line). Total damage of the first three layers is achieved at $t = 1$ s and can be seen in Fig. 5.

Table 1: Parameters of the cohesive zones.

Property	Bulk		Interfaces
	Al_2O_3	MgO	
K_{nn} [N/mm³]	$1 \cdot 10^9$		
K_{ss} [N/mm³]	1		$1 \cdot 10^9$
σ_n^c [MPa]	{60, <u>120</u>}	{60, 80, 100, <u>120</u>}	{60, <u>120</u>}
σ_s^c [MPa]			{<u>30</u>, 50}
G^c [N/mm]	0.15		{0.05, <u>0.15</u>, 0.25}

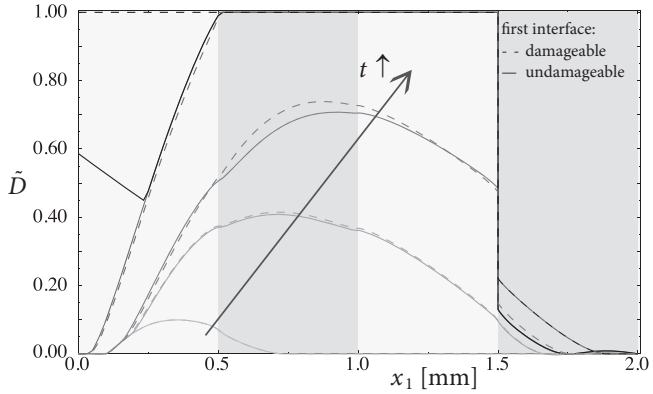

Fig. 5: Influence of the first interface's damage on damage $\tilde{D}(x_1)$ at different times $t \in \{0.001, 0.005, 0.008, 0.1, 1\}$s due to $T = 700$ K.

The influence of interface shear strength $\sigma_s^{cI} \in \{30, 50\}$ MPa on crack growth through the layers is shown in Figs. 6 and 7. It can be seen that a higher interface shear strength leads to less damage $\tilde{D}(x_1)$.

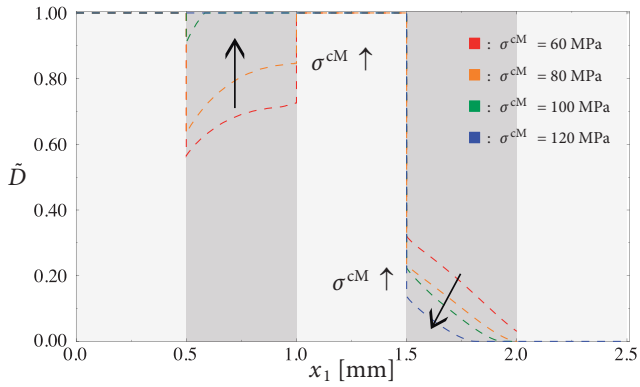

Fig. 6: Influence of the bulk strength of MgO $\sigma^{cM} \in \{60, 80, 100, 120\}$ MPa (interface: ($\sigma_s^{cI} = 30$ MPa) on damage $\tilde{D}(x_1)$ at $t = 1$ s due to $T = 700$ K.

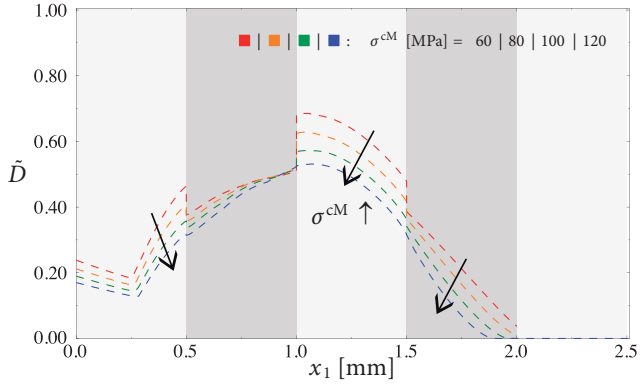

Fig. 7: Influence of the bulk strength of MgO $\sigma^{cM} \in \{60, 80, 100, 120\}$ MPa (interface: $\sigma_s^{cI} = 50$ MPa) on damage $\tilde{D}(x_1)$ at $t = 1$ s due to $T = 700$ K.

In this study, the bulk strength along x_1 is also varied by decreasing the MgO strength $\sigma^{cM} \in \{60, 80, 100, 120\}$ MPa, while the strength of Al_2O_3 is fixed to be $\sigma^{cA} = \sigma_n^{cA} = \sigma_s^{cA} = 120$ MPa. Choosing the shear strength of the interfaces to be $\sigma_s^{cI} = 30$ MPa results in almost total failure of the first three layers as shown in Figs. 5 and 6. In this case, the decrease in the MgO bulk strength σ^{cM} results in just a total failure of the first and third layer, but no longer of layer 2. With increasing strength σ^{cM} of the MgO, $\tilde{D}$ increases in the second layer (first MgO-layer) and decreases in the second MgO-layer (black arrows in Fig. 6), while stronger MgO leads to less damage in all layers for $\sigma_s^{cI} = 50$ MPa, which is also highlighted by the black arrows in Fig. 7.

Figs. 8, 9 and 10 show the damage variable along the coordinate x_2 of the first three interfaces. The fourth interface never fails, i.e. the cohesive contact is neglected there.

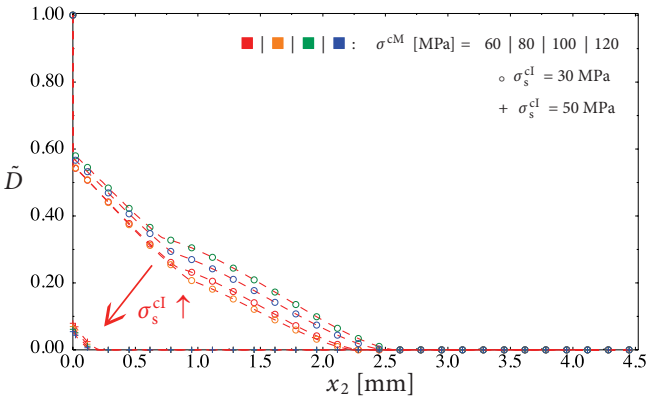

Fig. 8: Influence of the MgO bulk strength $\sigma^{cM} \in \{60, 80, 100, 120\}$ MPa and interface shear strength $\sigma_s^{cI} \in \{30, 50\}$ MPa on damage $\tilde{D}(x_2)$ of the first interface at $t = 1$ s.

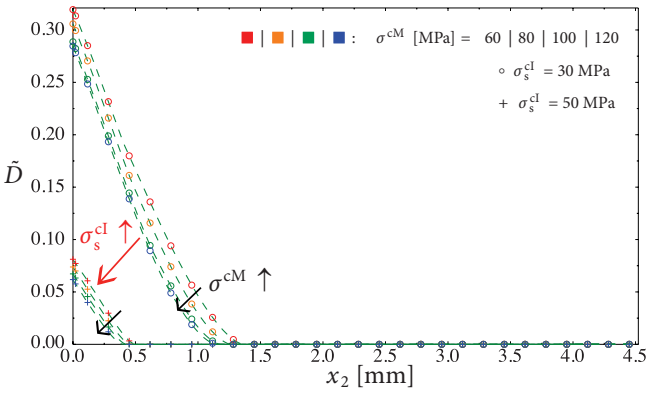

Fig. 9: Influence of the MgO bulk strength $\sigma^{cM} \in \{60, 80, 100, 120\}$ MPa and interface shear strength $\sigma_s^{cI} \in \{30, 50\}$ MPa on damage $\tilde{D}(x_2)$ of the second interface at $t = 1$ s.

A look at the first three interfaces in Figs. 8, 9 and 10 shows clearly the influence of the shear strength σ_s^{cI} in these interfaces on $\tilde{D}(x_2)$. Higher σ_s^{cI} values result in less interface damage (red arrows).

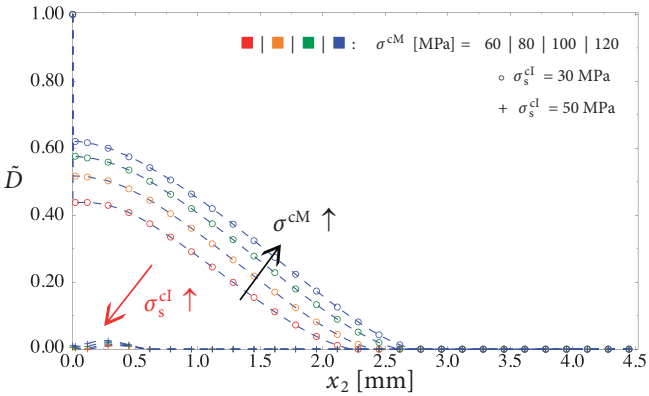

Fig. 10: Influence of the MgO bulk strength $\sigma^{cM} \in \{60, 80, 100, 120\}$ MPa and interface shear strength $\sigma_s^{cI} \in \{30, 50\}$ MPa on damage $\tilde{D}(x_2)$ of the third interface at $t = 1$ s.

The effect of the bulk strength σ^{cM} in MgO on the damage of the interfaces is not uniform for all interfaces. While $\tilde{D}(x_2)$ is decreased for increased σ^{cM} in the second interface, the damage behaves contrarily in the third interface (black arrows) and seems to be influenced randomly by the bulk strength of MgO in the first interface.

If the interface normal strength is decreased to $\sigma_n^{cI} = 60$ MPa compared to $\sigma_n^{cI} = 120$ MPa in the studies before, the damage along the symmetry plane in the bulk is almost not affected. Finally, the influence of the interface cohesive energy $G^{cI} \in \{0.05, 0.15, 0.25\}$ N/mm on the bulk damage $\tilde{D}(x_1)$ is examined. A higher G^c means a larger separation δ^f at total failure $\tilde{D} = 1$ of the cohesive contact, if K and the cohesive strength σ^c are kept constant.

Fig. 11 shows the influence of G^{cI} and MgO strength $\sigma^{cM} \in \{60,80,100, 120\}$ MPa on $\tilde{D}(x_1)$ for interface shear strength $\sigma_s^{cI} = 30$ MPa.

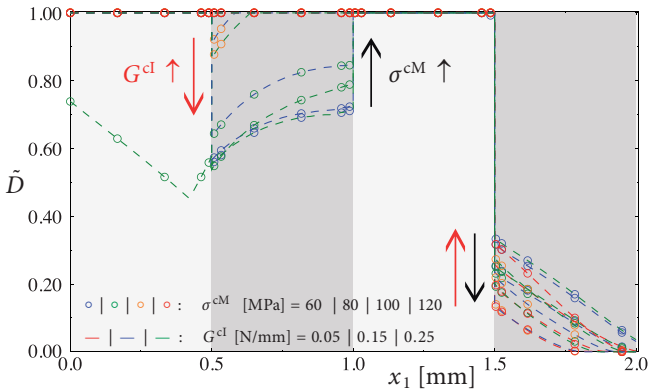

Fig. 11: Influence of the $G^{cI} \in \{0.05, 0.15, 0.25\}$ N/mm on the bulk damage $\tilde{D}(x_1)$ at $t = 1$ s due to $\bar{T} = 700$ K (interface: $\sigma_s^{cI} = 30$ MPa).

Thereby, with an increase in G^{cI}, less damage in the second layer and higher damage in the fourth layer are obtained.

In case of higher interface shear strength $\sigma_s^{cI} = 50$ MPa, G^{cI} has nearly no influence on $\tilde{D}(x_1)$ for the studied cohesive energies of $G^{cI} \in \{0.05, 0.15, 0.25\}$ N/mm and bulk strength $\sigma^{cM} \in \{60, 80,100,120\}$ MPa in MgO.

IV. Conclusions

A symmetrically layered strip and its damage evolution through the layers and along the interfaces caused by one-sided thermal shock of $\Delta T = 700$ K are studied. Because of the thermal stress distribution, a mode I crack propagation through the bulk material of the layers is assumed. This study is focused on the influence of the interfaces on this crack propagation and crack branching into the interfaces. Therefore, the possible crack paths through the layers and along the interfaces are modeled by using cohesive contact in the FE-program Abaqus. The damage value provided by Abaqus needs to be reformulated in order to have a damage value based on the cohesive strength as written in equation (7) instead of imaginary values as shown in equation (6).

With systematic variation of the cohesive properties, the damage evolution is calculated until the thermal steady state is achieved. It can be seen that the interface shear strength has the main effect on crack propagation. With decreased shear strength, damage along the interfaces increases and leads even to total failure of the first three layers. Moreover, a reduced MgO bulk strength (in comparison to Al_2O_3) causes higher damage values through the neighboring Al_2O_3 layers.

The cohesive energy G^{cI} influences crack propagation mainly for lower shear strength of the interfaces. Its effect on damage can be neglected for higher shear strength.

Because shear mode II dominated crack opening along the interfaces, the variation of the normal strength in the interfaces does not have any influence on the damage through the layers either.

The results of this study are not valid for every layered structure or every thermo-mechanical boundary value problem. Each structure and loading situation has to be investigated on its own. Regarding an optimization of thermal shock resistance, not just the number of layers, their thicknesses and material properties need to be determined, the cohesive parameters of the interfaces and bulk materials are also important properties of interest. This makes optimization very complex and time consuming.

V. Acknowledgement

The financial support of these investigations by the German Research Foundation (DFG) under contract KU929/16–2 within the Priority Program SPP 1418 "FIRE" is gratefully acknowledged.

References

1 Hein, J., Scheithauer, U., Haderk, K., Kuna, M., Michaelis, A.: Prospects of a new generation of refractories made by ceramic multilayer technology, *Refractories Manual*, **2**, 91–95, (2012).

2 Lemaitre, J.: Conditions of crack arrest by interfaces. In: Proceedings of the IUTAM Symposium held in Cambridge, U.K., 3-7 September 1995.

3 Clegg, W.J., Kendall, K., Alford, N. McN., Button, T.W., Birchall, J.D.: A simple way to make tough ceramics, *Nature*, **347**, 455–457, (1990).

4 Davis, J.B., Kristoffersson, A., Carlstroem, E., Clegg, W.J.: Fabrication and crack deflection in ceramic laminates with porous interlayers, *J. Am. Ceram. Soc.*, **83**, 2369–2374, (2000).

5 Pavlacka, R., Bermejo, R., Chang, Y., Green, D.J., Messing, G.L.: Fracture behavior of layered alumina microstructural composites with highly textured layers, *J. Am. Ceram. Soc.*, **96**, 1577–1585, (2013).

6 Harmer, M.P., Chan, H.M., Miller, G.A.: Unique opportunities for microstructural engineering with duplex and laminar ceramic composites, *J. Am. Ceram. Soc.*, **75**, [7], 1715–1728, (1992).

7 Russo, C.J., Harmer, M.P., Chan, H.M., Miller, G.A.: Design of laminated ceramic composite for improved strength and toughness, *J. Am. Ceram. Soc.*, **75**, [12], 3396–4000, (1992).

8 Lakshminarayanan, R., Shetty, D.K.: Toughening of layered ceramic composites with residual surface compression, *J. Am. Ceram. Soc.*, **79**, [1], 79–87, (1996).

9 Clegg, W.J.: Design of ceramic laminates for structural applications, *Mater. Sci. Tech.*, **14**, 483–495, (1998).

10 Rao, M.P., Roedel, J., Lange, F.F.: Residual stress induced R-curves in laminar ceramics that exhibit a threshold strength, *J. Am. Ceram. Soc.*, **84**, [11], 2722–2724, (2001).

11 Sglavo, V.M., Paternoster, M., Bertoldi, M.: Tailored residual stresses in high reliability alumina-mullite ceramic laminates, *J. Am. Ceram. Soc.*, **88** [10], 2826–2832, (2005).

[12] Sglavo, V. M., Bertoldi, M.: Design and production of ceramic laminates with high mechanical resistance and reliability, *Acta Mater.*, **54**, [18], 4929 – 4937, (2006).

[13] Lube, T., Pascual, J., Chalvet, F., Portu, G.: Effective fracture toughness in Al_2O_3 – Al_2O_3/ZrO_2 laminates, *J. Eur. Ceram. Soc.*, **27**, 1449 – 1453, (2007).

[14] Pascual, J., Lube, T., Danzer, R.: Fracture statistics of ceramic laminates strengthened by compressive residual stresses, *J. Eur. Ceram. Soc.*, **28**, [8], 1551 – 1556, (2008).

[15] Sglavo, V.M., Bertoldi, M.: Ceramic laminates with high mechanical reliability by design. mechanical properties and performance of engineering ceramics and Composites: A collection of papers presented at the 29th International Conference on Advanced Ceramics and Composites, Jan 23 – 28, 2005, Cocoa Beach, FL, *Ceram. Eng. Sci. Proc.*, **26**, [2], 363 – 370, (2009).

[16] Hein, J., Kuna, M.: Optimal design of layered refractories for thermal shock resistance. In: ECCOMAS 2012 – European Congress on Computational Methods in Applied Sciences and Engineering, e-Book Full Papers, 4511 – 4524, (2012).

[17] Ševeček, O., Kotoul, M., Leguillon, D., Martin, E., Bermejo, R.: Understanding the edge crack phenomenon in ceramic laminates, *Fract. Struct. Integrity*, **0**, [34], 362 – 370, (2015).

[18] Bermejo, R., Torres, Y., Sánchez-Herencia, A.J., Baudín, C., Anglada, M., Llanes, L.: Residual stresses, strength and toughness of laminates with different layer thickness ratios, *Acta Mater.*, **54**, [18], 4745 – 4757, (2006).

[19] Bermejo, R., Baudín, C., Moreno, R., Llanes, L., Sánchez-Herencia, A.J.: Processing optimisation and fracture behaviour of layered ceramic composites with highly compressive layers, *Compos. Sci. Tech.*, **67**, [9], 1930 – 1938, (2007).

[20] Hutchinson, J.W., Suo, Z.: Mixed mode cracking in layered materials, *Adv. App. Mech.*, **29**, 63 – 191, (1992).

[21] Zhang, W., Telle, R., Uebel, J.: R-curve behaviour in weak interface-toughened SiC-C laminates by discrete element modelling, *J. Eur. Ceram. Soc.*, **34**, 217 – 227, (2014).

[22] Oechsner, M., Hillman, C., Lange, F.F.: Crack bifurcation in laminar ceramic composites, *J. Am. Ceram. Soc.*, **79**, 1834 – 1838, (1996).

[23] Hbaieb, K., McMeeking, R.M., Lange, F.F.: Crack bifurcation in laminar ceramics having large compressive stress, *Int. J. Solids Struct.*, **44**, [10], 3328 – 3343, (2007).

[24] Bermejo, R., Danzer, R.: High failure resistance layered ceramics using crack bifurcation and interface delamination as reinforcement mechanisms, *Eng. Fract. Mech.*, **77** [11], 2126 – 2135, (2010).

[25] Chen, C.R., Bermejo, R., Kolednik, O.: Numerical analysis on special cracking phenomena of residual compressive inter-layers in ceramic laminates, *Eng. Fract. Mech.*, **77** [13], 2567 – 2576, (2010).

[26] Náhlík, L., Stegnerová, K., Hutař, P.: Estimation of stepwise crack propagation in ceramic laminates with strong interfaces, *Frattura ed Integrità Strutturale*, **34**, 137 – 145, (2015).

[27] Evans, A.G., Mumm, D.R., Hutchinson, J.W., Meier, G.H., Pettit, F.S.: Mechanisms controlling the durability of thermal barrier coatings, *Prog. Mater. Sci.*, **46**, [5], 505 – 553, (2001).

[28] Hutchinson, J.W., Evans, A.G.: On the delamination of thermal barrier coatings in a thermal gradient, *Surf. Coat. Tech.*, **149**, [2 – 3], 179 – 184, (2002).

[29] Chen, X., Hutchinson, J.W., He, M.Y., Evans, A.G.: On the propagation and coalescence of delamination cracks in compressed coatings: with application to thermal barrier systems, *Acta Mater.*, **51** [7], 2017 – 2030, (2003).

[30] Xu, T., He, M.Y., Evans, A.G.: A numerical assessment of the durability of thermal barrier systems that fail by ratcheting of the thermally grown oxide, *Acta Mater.*, **51**, [13], 3807 – 3820, (2003).

[31] He, M.Y., Hutchinson, J.W., Evans, A.G.: Simulation of stresses and de-lamination in a plasma-sprayed thermal barrier system upon thermal cycling, *Mater. Sci. Eng.: A*, **345**, [1 – 2], 172 – 178, (2003).

[32] Chen, X., Wang, R., Yao, N., Evans, A.G., Hutchinson, J.W., Bruce, R.W.: Foreign object damage in a thermal barrier system: mechanisms and simulations, *Mater. Sci. Eng.: A*, **352**, [1 – 2], 221 – 231, (2003).

[33] He, M.Y., Mumm, D.R., Evans, A.G.: Criteria for the delamination of thermal barrier coatings: with application to thermal gradients, *Surf. Coat. Tech.*, **185**, [2 – 3], 184 – 193, (2004).

[34] Evans, A.G., Hutchinson, J.W.: The mechanics of coating delamination in thermal gradients, *Surf. Coat. Tech.*, **201**, [18], 7905 – 7916, (2007).

[35] Krämer, S., Faulhaber, S., Chambers, M., Clarke, D.R., Levi, C.G., Hutchinson, J.W., Evans, A.G.: Mechanisms of cracking and delamination within thick thermal barrier systems in aero-engines subject to calcium-magnesium-alumino-silicate (CMAS) penetration, *Mater. Sci. Eng.: A*, **490**, [1 – 2], 26 – 35, (2008).

[36] Yang, L., Zhou, Y.C., Lu, C.: Damage evolution and rupture time prediction in thermal barrier coatings subjected to cyclic heating and cooling: an Acoustic emission method, *Acta Mater.*, **59**, [17], 6519 – 6529, (2011).

[37] Fleck, N.A., Cocks, A.C.F., Lampenscherf, S.: Thermal shock resistance of air plasma sprayed thermal barrier coatings, *J. Eur. Ceram. Soc.*, **34**, [11], 2687 – 2694, (2014).

[38] Kim, M.-S., Myoung, S.-W., Lu, Z., Lee, J.-H., Jung, Y-G., Choi, B.-G., Kim, I.-S., Cho, C.-Y.: Thermal durability of thermal barrier coatings with layered bond coat in cyclic thermal exposure, *J. Ceram. Soc. Japan*, **122**, [12], 982 – 988, (2014).

[39] Nayebpashaee, N., Seyedein, S.H., Aboutalebi, M.R., Sarpoolaky, H., Hadavi, S.M.M.: Finite element simulation of residual stress and failure mechanism in plasma sprayed thermal barrier coatings using actual microstructure as the representative volume, *Surf. Coat. Tech.*, **291**, 103 – 114, (2016).

[40] Hein, J., Kuna, M.: Optimizing thermal shock resistance of layered refractories, *Adv. Eng. Mater.*, **14**, 408 – 415, (2012).

[41] Hein, J., Storm, J., Kuna, M.: Numerical thermal shock analysis of functionally graded and layered materials, *Int. J. Therm. Sci.*, **60**, 41 – 51, (2012).

[42] Kuna, M.: Finite elements in fracture mechanics – theory – numerics – applications. Springer Netherlands, Dordrecht, 2013.

[43] Schwalbe, K.-H., Scheider, I., Cornec, A.: Guidelines for applying cohesive models to the damage behaviour of engineering materials and structures, Springer-Verlag, Berlin Heidelberg, 2013.

[44] Abaqus 6.12 – 3. Abaqus/CAE User's Manuel, ©Dassault Systemes, 2012.

[45] Roth, S.: Development and implementation of cyclic cohesive zone models for the simulation of material fatigue (in German), Dissertation, TU Bergakademie, Freiberg, 2015.